Journal of Materials Chemistry A

COMMUNICATION

View Article Online
View Journal | View Issue

Cite this: J. Mater. Chem. A, 2017, 5, 3172

Received 20th January 2017
Accepted 26th January 2017

DOI: 10.1039/c7ta00679a

rsc.li/materials-a

Improving the activity and stability of Ir catalysts for PEM electrolyzer anodes by SnO_2:Sb aerogel supports: does V addition play an active role in electrocatalysis?†

Li Wang,[a] Feihong Song,[a] Guillaume Ozouf,[b] Dorin Geiger,[c] Tobias Morawietz,[d] Michael Handl,[d] Pawel Gazdzicki,[a] Christian Beauger,[b] Ute Kaiser,[c] Renate Hiesgen,[d] Aldo S. Gago*[a] and K. Andreas Friedrich*[ae]

Low Ir loading oxygen evolution reaction (OER) catalysts with superior activity and durability for proton exchange membrane (PEM) electrolyzers are an important topic in industry and academia. One possible strategy for addressing this challenge is the use of support materials that are stable under highly corrosive acidic environments at a high working potential (>1.4 V). Moreover, highly porous structure is another key criteria for OER catalyst support to achieve a high electrochemical surface area. Here, we report a novel Ir supported on a SnO_2:Sb aerogel OER catalyst (Ir/SnO_2:Sb-mod-V), which was prepared under ambient pressure by using vanadium additives. It shows an unrivaled activity and enhanced stability, on which vanadium does not play any active role but demonstrates the influences that changes the porosity of the aerogel support and affects the impurity content of the chlorine. By taking advantage of the high porosity of the aerogel substrate, Ir/SnO_2:Sb-mod-V allows a decrease of more than 70 wt% for precious metal usage in the catalyst layer while keeping a similar OER activity compared to its unsupported counterpart.

PEM electrolyzers have attracted great attention as a promising technology to store intermittent electricity from solar or wind energy in the last decade. To date, Ir-based electrocatalysts are still the only technically feasible option as an anode catalyst to promote the oxygen evolution reaction (OER) because they combine both high activity and considerable stability.[1] However, a large amount of Ir (3–0.5 mg cm^{-2}) is necessary, compared to less than 0.3 mg cm^{-2} of Pt on the cathode side, to overcome the sluggish OER reaction kinetics, which lowers the efficiency of the electrolyzer.[1,2] Considering the high cost and scarcity of Ir, extensive research has been performed to address this challenge.[3–7]

Recently, two main strategies were used for reducing the Ir loading: (i) developing highly active amorphous IrO_x based catalysts and (ii) using an electro-conductive ceramic as a substrate material.[3,4] Regarding the first strategy, Cherevko *et al.* and Danilovic *et al.* investigated amorphous IrO_x films on Ir; they showed higher activities than annealed IrO_2 layers, yet a higher dissolution rate.[8,9] Nanoparticles of IrO_x–Ir and Ir-black also show much higher activities compared to state-of-the-art thermally treated IrO_2.[7] Markovic and co-workers reported one $IrRuO_x$ electrocatalyst with improved stability due to the segregation of the Ir into Ir nano-domains by annealing the catalyst.[10] Seitz *et al.* developed an IrO_x/$SrIrO_3$ catalyst by leaching Sr from the surface of $SrIrO_3$, outperforming even RuO_x systems.[3]

By taking the second approach, our group demonstrated improved Ir utilization compared to Ir-black by depositing metallic Ir nano-particles on Magnéli phase Ti_4O_7 without further thermal treatment.[6] Chen *et al.* also reported an amelioration for the OER in acidic medium when using Ti_4O_7 as a support for Ir-based catalysts.[11] In recent years, the well-known electro-ceramic tin oxide doped with antimony (SnO_2:Sb) has attracted significant attention from the research community due to its considerable electronic conductivity and high electrochemical stability.[12–14] Puthiyapura *et al.* prepared and investigated the rutile phase of IrO_2 supported on commercial SnO_2:Sb particles, showing improved Ir utilization.[15] In addition, Strasser and co-workers developed a highly active catalyst consisting of $IrNiO_x$ supported on mesoporous SnO_2:Sb and revealed a metal/metal oxide support interaction (MMOSI) between amorphous IrO_x and SnO_2:Sb, resulting in an enhancement of the intrinsic OER activity.[4,16]

[a]Institute of Engineering Thermodynamics, German Aerospace Center (DLR), Pfaffenwaldring 38-40, 70569 Stuttgart, Germany. E-mail: aldo.gago@dlr.de; andreas.friedrich@dlr.de

[b]MINES ParisTech, PSL Research University, PERSEE-Centre procédés énergies renouvelables et systems énergétiques, CS 10207, Rue Claude Daunesse, 06904 Sophia-Antipolis Cedex, France

[c]Group of Electron Microscopy of Materials Science, Central Facility for Electron Microscopy, University of Ulm, 89081 Ulm, Germany

[d]University of Applied Sciences Esslingen, Dep. of Basic Science, Kanalstrasse 33, Esslingen, 73728, Germany

[e]Institute of Energy Storage, University of Stuttgart, Pfaffenwaldring 31, 70569 Stuttgart, Germany

† Electronic supplementary information (ESI) available: Materials and methods, energy-dispersive X-ray spectroscopy (EDS) analysis, additional XPS, SEM, HRTEM and electrochemical measurements results. See DOI: 10.1039/c7ta00679a

The precious metal utilization and stability of nanostructured Ir anodes of PEM electrolyzers have yet to be further improved, the aforementioned efforts notwithstanding. In this context, three-dimensional (3D) aerogel structures of carbon[17] and SnO_2:Sb[18] are widely studied as catalyst supports for the oxygen reduction reaction (ORR) due to their ultra-high intrinsic specific surface area. In the present work, we develop an iridium supported on a SnO_2:Sb aerogel catalyst (Ir/SnO_2:Sb-mod-V) for OER with well-retained highly porous structure by using V additives during synthesis, showing an unprecedented activity concurrent with an excellent stability compared to Ir/SnO_2:Sb and unsupported IrO_x. The retained porosity of aerogel substrate after synthesis yields an increased electrochemical surface area, which is directly correlated with catalyst performance. Previous works have reported that vanadium can enhance the electrocatalyst performance either by forming M–V (M is precious metal) alloy[19–21] or by surface vanadium redox species modification.[22,23] However, our results demonstrate that vanadium species are not an active part for OER, rather showing the significant influences on retaining the aerogel structure under atmospheric drying and lowering the impurity content of the chlorine. To the best of our knowledge, we present for the first time the exploitation of the highly porous 3D structure of aerogel support for enhancing OER activity. The synthesized catalysts were characterized by X-ray photoelectron spectroscopy (XPS), scanning electron microscope (SEM), energy-dispersive X-ray spectroscopy (EDS), high-resolution transmission electron microscopy (HRTEM) and atomic force microscopy (AFM). Cyclic voltammetry (CV), chronopotentiometry and copper underpotential deposition (Cu-UPD) were carried out to evaluate the performance and stability of the catalysts.

An aerogel of SnO_2:Sb was formed by drying a previously synthesized gel using a sol–gel route from metal alkoxide precursors in supercritical conditions.[24] Nanoparticles of Ir were reduced under an Ar atmosphere, according to the previously reported synthesis,[6] and deposited on the aerogel substrate. In the case of Ir/SnO_2:Sb-mod-V, an ammonium metavanadate (NH_4VO_3) was introduced after the addition of the surfactant cetyltrimethylammonium bromide (CTAB) to the solvent. Unsupported IrO_x was achieved by the same method without adding the SnO_2:Sb aerogel. All the prepared catalysts were used without further thermal treatment, avoiding the formation of the IrO_2 rutile phase, which shows lower OER activity than the amorphous IrO_x produced *via* electrochemical oxidation.[9]

Using XPS analysis, shown in Fig. 1, vanadium was clearly identified in the Ir/SnO_2:Sb-mod-V sample. According to the elemental composition profile depicted in Fig. 1a, the atomic concentration of vanadium was 3–4 at%, which was approximately 3 times less than the concentration of iridium, corresponding to a wt% Ir : V ratio of approximately 10 : 1. It is worth mentioning that 30 wt% of V (*vs.* IrV) was calculated as the nominal ratio (atomic V : Ir ratio of approximately 1.6 : 1) for the synthesis, which is much higher than the content detected by XPS, meaning that more than half of V was not reduced and rinsed away afterwards.

The elemental composition profile of Ir/SnO_2:Sb, depicted in Fig. 1b for comparison, exhibits very similar elemental concentrations, but with no vanadium (see ESI†), a slightly

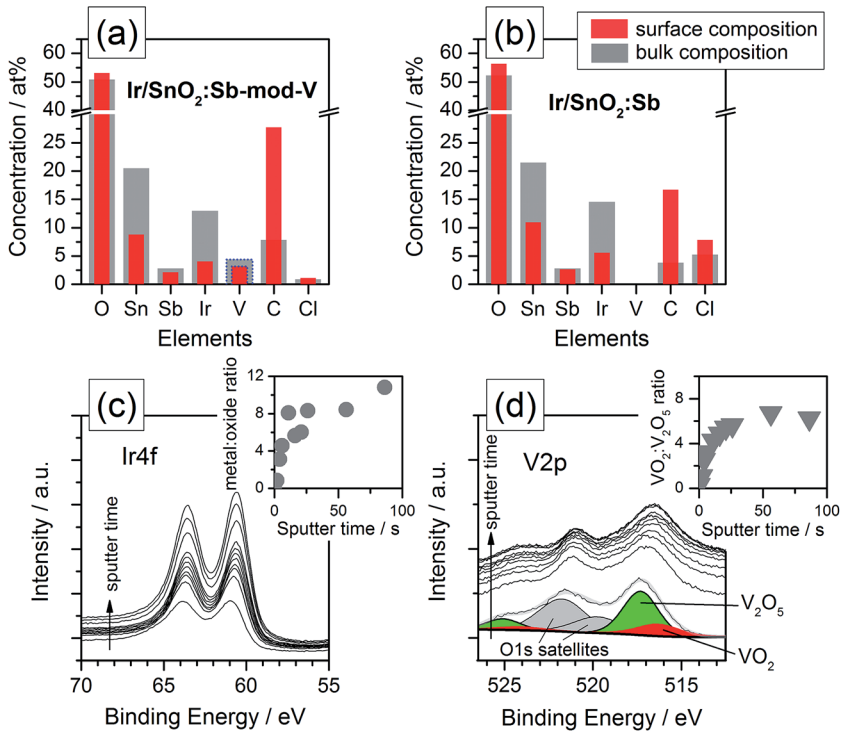

Fig. 1 XPS analysis: surface and bulk element composition profiles of (a) Ir/SnO_2:Sb-mod-V and (b) Ir/SnO_2:Sb. Panels (c) and (d) show detailed Ir4f and V2p spectra, respectively. In the insets of panels (c) and (d), the respective atomic ratios of Ir-metal : Ir-oxide and VO_2 : V_2O_5 are plotted.

reduced carbon signal that was detected predominantly on the sample surface. In both cases, the samples were dominated by Sn and O. The bulk Sn : O ratio equals 0.4, which was slightly lower than the expected stoichiometric ratio of the SnO_2 support material. The additional O could be due to additional oxidized components or possibly contamination. It is worth to mention that the Cl^- contaminates show an apparent increase in the sample of Ir/SnO_2:Sb, 5.25 at% compared to 0.88 at% of Ir/SnO_2:Sb-mod-V, which normally has a strong negative effect on precious metal electrocatalysts.[25,26] This change is ascribed to NH_4VO_3 additions during synthesis, $NaBH_4$ shows a more powerful reducing properties when V species present in the reaction solution, resulting in a different residual Cl^- content.

The Ir composition, obtained by peak fitting of the Ir4f detailed spectra shown in Fig. 1c, is depicted in the inset. Apparently, the surface iridium was fully oxidized, while the metal : oxide ratio increased to 8–10 for the bulk ($t_{sputter}$ > 20 s). Vanadium was detected by measuring the V2p orbital spectra. To discriminate between the V2p peaks and overlapping O1s satellite peaks, the fitted signals before sputtering were added in Fig. 1d (see also ESI†). According to the fitted $V2p_{3/2}$ levels at peak positions at 516.4 and 517.3 eV, the corresponding vanadium species has been identified as VO_2 and V_2O_5; no metallic vanadium was detected, which was expected between 512–513 eV.[27,28] The ratio profile of the vanadium-oxide species, provided as an inset, shows that V_2O_5 clearly dominates at the sample surface, but mainly VO_2 was found to occur in the bulk.

EDS combined with SEM was used for the elemental distribution analysis to analyze the presence of vanadium and chlorine impurity further. The results (Table S2†) show the wt% ratio of Ir : V equals approx. 10 : 1 in the sample of Ir/SnO_2:Sb-mod-V, in agreement with the XPS measurements described above. Ir/SnO_2:Sb was also analyzed under the same conditions for comparison purposes (Table S3†), and the absence of the V signals indicates that the V observed on Ir/SnO_2:Sb-mod-V was indeed derived from the precursor NH_4VO_3. Chlorine impurity changes shows the same trend as observed from XPS, *ca.* 5 times higher in the case of Ir/SnO_2:Sb.

The morphology of the Ir/SnO_2:Sb-mod-V was analyzed with SEM by using the secondary electron as shown in Fig. 2a (also Fig. S2(b), see ESI†). By comparison with the original SnO_2:Sb aerogel (Fig. S2(a), see ESI†), the highly porous structure of aerogel was retained after Ir deposition when the V compounds were present on its surface. Clearly, the highly porous structure of Ir/SnO_2:Sb was damaged in the samples without V, as apparent from the dense (Fig. S2(c), see ESI†), flat (Fig. S3(d),† low resolution) morphologic surface. One plausible explanation is that the vanadium compounds, either VO_2 or V_2O_5, reduce the surface tension of the ethanol solution, thereby also reducing the capillary pressure force during the atmospheric drying of the catalyst. It has been reported that replacing a high surface tension solvent with a low surface tension solvent leads to the retention of the 3D cross-linked structure of aerogels during atmospheric drying.[29] The corresponding back scattered electron SEM images (Fig. S3(a) and (c), see ESI†) show a uniform Ir dispersion on both Ir/SnO_2:Sb-mod-V and Ir/SnO_2:Sb on a larger scale, in which Ir particles are present as bright tiny spots.

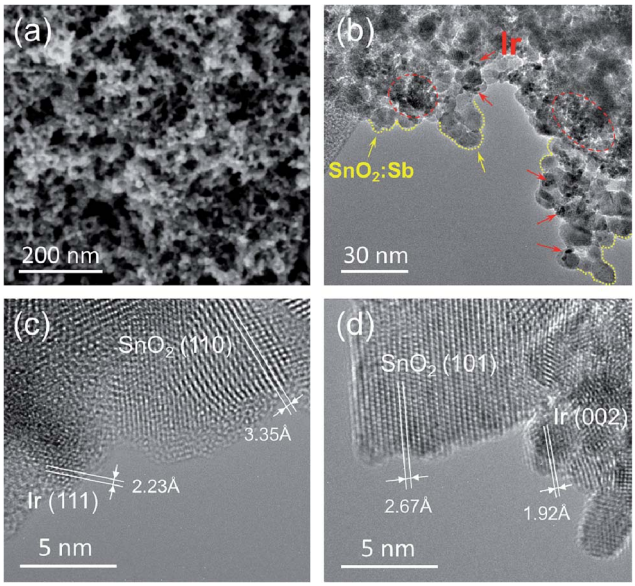

Fig. 2 (a) SEM image of Ir/SnO_2:Sb-mod-V; (b, c) 300 kV aberration-corrected HRTEM images of Ir/SnO_2:Sb-mod-V at different magnifications, SnO_2:Sb particles are lined with yellow, while Ir-containing areas are marked in red; (d) 300 kV aberration-corrected HRTEM image of Ir/SnO_2:Sb.

Fig. 2b shows the HRTEM image of Ir/SnO_2:Sb-mod-V. Particles, such as those surrounded by yellow dashed lines, with a size of *ca.* 10 nm were identified as a single particle of SnO_2:Sb aerogel. The small dark particles, indicated by red circles and arrows, were attributed to Ir nano-particles with a smaller particle size of *ca.* 2–3 nm. As we can see, some of the Ir particles were situated on the substrate as single particles and were well-dispersed on the aerogel structure, while some show agglomeration as illustrated in the red circle of Fig. 2b. One selected area of the Ir/SnO_2:Sb-mod-V is shown in Fig. 2c at higher magnification, where a single Ir particle is next to SnO_2:Sb particles. Crystallographic analysis enabled the (111) lattice plane of the Ir nano-particles and the (110) lattice plane of the SnO_2 particles to be discerned. Interestingly, no evidence of V was found at the nano-scale, as shown in Fig. 2b and c, which implies that Ir and V did not form a solid solution and that the V was distributed heterogeneously in the sample of Ir/SnO_2:Sb-mod-V. For comparison, a HRTEM image of Ir/SnO_2:Sb is shown in Fig. 2d. As expected, Ir and SnO_2:Sb were recognized based on the Ir (002) lattice plane and the SnO_2 (101) lattice, with characteristic distances of 1.92 Å and of 2.67 Å, respectively. A similar structure of Ir/SnO_2:Sb-mod-V and Ir/SnO_2:Sb at the nano-scale indicates that the presence of V had no significant influence on the microstructure of the Ir catalysts supported on SnO_2:Sb.

Electronic conductivity, which normally influences performance, is an important parameter for evaluating electrocatalysts. An AFM conductivity measurement was carried out for this purpose. Two SnO_2:Sb aerogel supported Ir catalysts were deposited on a Si wafer and electrically connected to the metal substrate with conductive silver paste. Fig. 3a and b show the

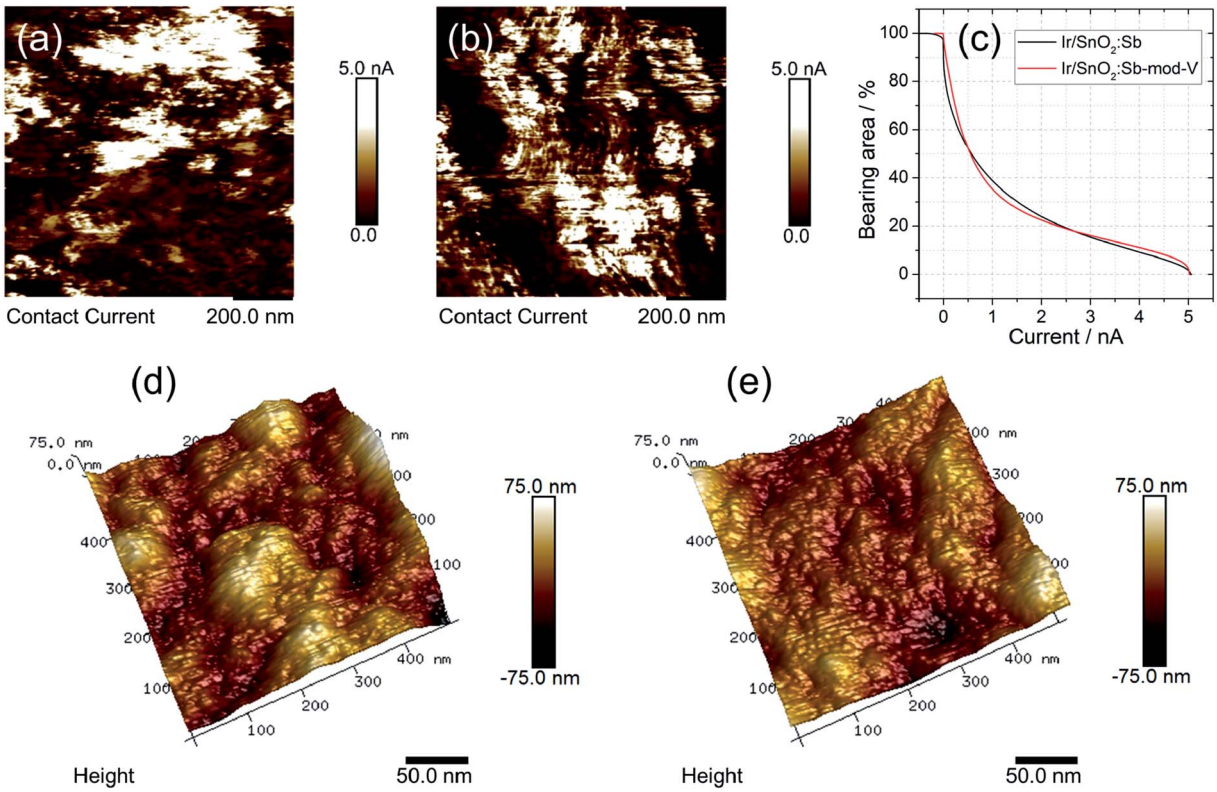

Fig. 3 AFM measurements: contact current mapping of (a) Ir/SnO_2:Sb-mod-V and (b) Ir/SnO_2:Sb; panel (c) shows the bearing area *vs.* current for the two supported catalysts, evaluated from AFM current mappings; 3D topography of (d) Ir/SnO_2:Sb-mod-V and (e) Ir/SnO_2:Sb.

current mapping of Ir/SnO_2:Sb-mod-V and Ir/SnO_2:Sb, respectively. The conductive area was (95 ± 4)% for Ir/SnO_2:Sb-mod-V and (91 ± 3)% for Ir/SnO_2:Sb. The magnitude of the conductive area percentage with a varied threshold current is shown in Fig. 3c. No significant difference in conductivity between Ir/SnO_2:Sb-mod-V and Ir/SnO_2:Sb was observed. Also a similar mean size of the conductive agglomerates was determined at ~28 nm for Ir/SnO_2:Sb-mod-V and ~27 nm for Ir/SnO_2:Sb.

Surface roughness can be an indicator for the porosity of powder samples. The porosity is another key parameter for evaluating electrocatalysts, especially OER catalysts, because the porosity influences water transport and the detachment of oxygen. For Ir/SnO_2:Sb-mod-V and Ir/SnO_2:Sb, the roughness (R_a) determined from three different spots on the samples at the 3 μm scale was (100 ± 20) nm for Ir/SnO_2:Sb-mod-V and (80 ± 20) nm for Ir/SnO_2:Sb. However, one should be aware of the large error bars, ±20 nm in both cases, and the importance of inter-agglomerate roughness. The mean error is a result of the heterogeneities of the samples at this scale. Note that the determination of (R_a) on a smaller area taking care that only the surface of one agglomerate is measured (evaluating 300 × 300 nm^2 areas) leads to a reduced roughness (16 ± 1 nm for Ir/SnO_2:Sb-mod-V and 12 nm ± 1 nm for Ir/SnO_2:Sb). It was, however, larger for the V-modified sample. In Fig. 3d and e, topography images of Ir/SnO_2:Sb-mod-V and Ir/SnO_2:Sb are given. Their difference in surface roughness implies that the 3D porous structure of Ir/SnO_2:Sb-mod-V was retained after synthesis, while the porous structure partially collapsed in the case of Ir/SnO_2:Sb. This was in agreement with the SEM morphology analysis.

Three catalysts were electrochemically oxidized by 10 cycles of CV between 0 V and 1.6 V *vs.* a reversible hydrogen electrode (RHE) (Fig. S7, see ESI†). Afterwards, 3 cycles of CV were carried out from 1.0 V to 1.6 V to examine OER activity. The first CV cycle after capacitance correction is shown in Fig. 4a. Both SnO_2:Sb aerogel supported Ir catalysts displayed significantly enhanced OER activity normalized by Ir loading compared to the unsupported IrO_x catalyst that we previously published.[7] Furthermore, Ir/SnO_2:Sb-mod-V exhibited slightly higher OER mass activity compared with Ir/SnO_2:Sb. Ir mass activity was compared at an overpotential of 280 mV (Fig. 4b), where mass transport effects were negligible. At this potential, unsupported IrO_x, Ir/SnO_2:Sb and Ir/SnO_2:Sb-mod-V reached 33.2 A g^{-1}, 94.6 A g^{-1} and 121.5 A g^{-1}, respectively. For comparison, IrO_x/com.-ATO and $IrNiO_x$/meso-ATO reported by Nong *et al.*,[4] reached *ca.* 32 A g^{-1} and 89 A g^{-1}, respectively. It is worthwhile to note that any comparison of mass activities is difficult because the measured values depend greatly on the electrode preparation method, the amount of ionomer in the catalyst layer, the electrolyte concentration, *etc.* Even so, the most significant result is the fact that the three catalysts showed similar geometric OER activity, while the supported samples contained only *ca.* 28 wt% Ir on the electrodes (Fig. S8, see ESI†), showing that the SnO_2:Sb aerogel support had successfully improved Ir utilization. In

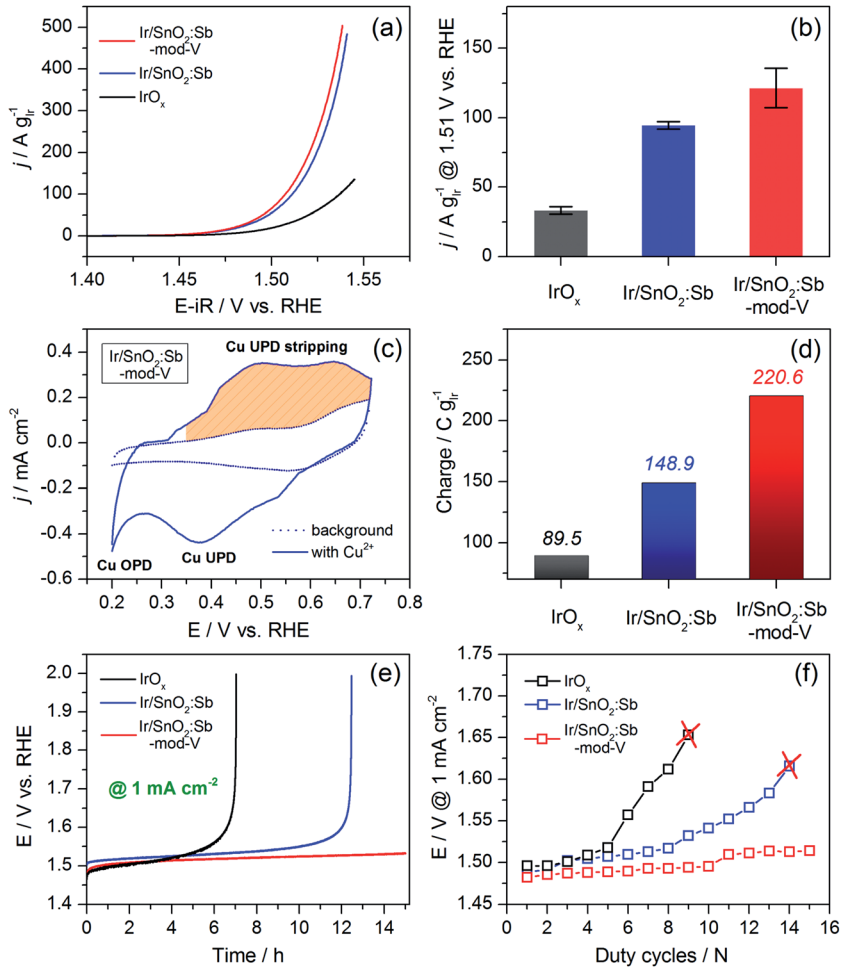

Fig. 4 (a) OER activity performance of Ir/SnO_2:Sb-mod-V, Ir/SnO_2:Sb and unsupported IrO_x, 25 °C, N_2-saturated 0.05 M H_2SO_4, 5 mV s^{-1}, 1600 rpm; (b) mass activity comparison under an overpotential of 280 mV; (c) Cu-UPD profile of Ir/SnO_2:Sb-mod-V; (d) charge comparison based on Cu-UPD stripping peaks among three catalysts; (e) stability tests: chronopotentiometry with a current density of 1 mA cm^{-2} for 15 hours, 25 °C, N_2-saturated 0.05 M H_2SO_4; (f) duty cycle measurements: the corresponding potential under 1 mA cm^{-2} after each duty cycle was recorded. Ir loading on electrodes: 60 μg cm^{-2} for IrO_x, 17 μg cm^{-2} for Ir/SnO_2:Sb-mod-V and Ir/SnO_2:Sb.

more practical terms, one can foresee that it is possible to retain high efficiencies with less than 70 wt% Ir loading in the membrane electrode assembly (MEA). In this context, the use of aerogel supports paves a way to develop ultra-low loading Ir anodes for PEM electrolyzers.

The Tafel slope of three catalysts are given in Table 1, 43.7 mV dec^{-1}, 41.8 mV dec^{-1} and 40.9 mV dec^{-1} for IrO_x, Ir/SnO_2:Sb and Ir/SnO_2:Sb-mod-V, respectively. The slight difference between supported catalysts and unsupported catalyst can be attributed to the influence from MMOSI.[16] Similar Tafel slope implies that three catalysts have the same active center, namely Ir, and V does not contribute to the OER catalysis in the case of Ir/SnO_2:Sb-mod-V. This is confirmed by XPS analysis on electrode surface (Fig. S10, ESI†) after electrochemical oxidation (seq. 1 and seq. 2 in Table S1†), a *ca.* 95 at% decrease of vanadium content strongly indicates that V is only a transient before catalyst electrochemical activation. It does not play any active role in OER catalysis, rather influencing the porosity of aerogel support and residual chlorine content.

Table 1 Tafel slope comparison

Catalyst	IrO_x	Ir/SnO_2:Sb	Ir/SnO_2:Sb-mod-V
Tafel slope (mV dec^{-1})	43.7	41.8	40.9

The catalyst particles of Ir/SnO_2:Sb-mod-V after 10 CV cycles of electrochemical oxidation (EC) were collected and analyzed by HRTEM. The image (Fig. S4, see ESI†) showed that Ir and SnO_2:Sb retained a similar size and structure, *ca.* 2 nm and 10 nm, respectively, compared to the fresh sample. This indicates that no significant changes, either for Ir particles or SnO_2:Sb particles, were observed after the EC protocol.

To further elucidate the OER activity difference among the three catalysts, a Cu-UPD measurement was performed to determine the charge during Cu-UPD stripping, which is related to the electrochemical surface area. Copper is a suitable choice for UPD on iridium because both elements have similar atomic radii: Cu (0.128 nm) and Ir (0.136 nm).[30] The integration of the

Cu-UPD stripping peak area analysis enables the calculation of the electrochemical surface area of Ir, supposing one copper atom adsorbed onto one surface iridium atom and that 2 electrons are transferred.[31] Fig. 4c shows the Cu-UPD profile of Ir/SnO_2:Sb-mod-V and its background CV curve measured in the same electrolyte without Cu^{2+}. The Cu-UPD peak appeared in the cathodic scan at *ca.* 0.38 V *vs.* RHE. This was followed by copper overpotential deposition (Cu-OPD) from *ca.* 0.25 V.[32] The anodic peak from 0.35 V to 0.72 V *vs.* RHE was attributed to the Cu-UPD stripping and used for evaluating the UPD charge; the values are provided in Fig. 4d.

Based on their Cu-UPD stripping peaks (Fig. S11, ESI†), a charge of 220.6 C g^{-1} relative to the Ir loading was observed for Ir/SnO_2:Sb-mod-V, whereas the charge for Ir/SnO_2:Sb and unsupported IrO_x was 148.9 C g^{-1} and 89.5 C g^{-1}, respectively. This result was in agreement with the Ir mass normalized OER activity under an overpotential of 280 mV, implying that the Cu-UPD stripping charge can be used as an indicator of the electrochemical surface area for metallic Ir-based OER catalysts.

Chronopotentiometry was used for evaluating the stability, presented in Fig. 4e. As we can see, the potential of unsupported IrO_x and Ir/SnO_2:Sb, under a constant current density of 1 mA cm^{-2}, increased sharply to 2.0 V *vs.* RHE after *ca.* 7 and 12 h, respectively. On the contrary, no significant potential increase was observed for Ir/SnO_2:Sb-mod-V during the 15 h test. The result demonstrates that the stability of the electrodes with supported catalysts was clearly promoted by using SnO_2:Sb aerogel substrate, and it was further enhanced in the case of Ir/SnO_2:Sb-mod-V due to its higher support porosity and less Cl^- contaminates, resulting in a higher accessible electrochemical surface area.

The stability of the catalysts were further confirmed by performing a "duty-cycle" protocol (details see ESI†), which was proposed by Strasser and co-workers to simulate PEM electrolyzer working conditions,[4] to provide a dynamic operation environment. The results are shown in Fig. 4f. Unsupported IrO_x and Ir/SnO_2:Sb completely lost their activities after 9 and 14 duty-cycles, respectively, while the overpotential of Ir/SnO_2:Sb-mod-V at 1 mA cm^{-2} increased only slightly after 15 duty-cycles, in agreement with the stability trend shown in Fig. 4e.

Based on the above investigation, the boosted OER activity and superior stability of Ir/SnO_2:Sb-mod-V can be explained by the following: (1) Ir utilization was significantly increased by using an aerogel structure as a support because of its 3D cross-linked porous structure, confirmed by Cu-UPD measurements; (2) possibly, the MMOSI between Ir and SnO_2:Sb additionally enhanced the OER;[16] (3) V compounds (VO_2 or V_2O_5), which present as a transient, help to retain the highly porous 3D structure of the aerogel and lower the chlorine impurity content, leading to a high electrochemical surface area.

In summary, conductive ceramic aerogel, SnO_2:Sb, has been introduced for the first time as OER catalyst supports for PEM electrolyzers, showing promising applications. The highly porous structure of SnO_2:Sb aerogel was successfully retained by using V additives under atmospheric drying. Ir/SnO_2:Sb-mod-V demonstrates an unprecedentedly improved Ir utilization and enhanced stability, which is attributed to its high porosity of aerogel substrate and low chlorine impurity content, resulting in a high accessible electrochemical surface area. V addition importantly influences the porosity of catalyst support and Cl^- contaminates content, but does not play any active role in OER catalysis. Chlorine-contained precursor should be avoided in future work to get rid of Cl^- contaminations. Further understanding of surface and electronic interactions between the SnO_2:Sb aerogel substrate and Ir active sites requires fine structure spectroscopies and in operando characterization techniques. These studies are part of our ongoing work. In addition, atomic layer deposition (ALD) method, which is a novel approach for preparing advanced Pt-based catalysts for PEM fuel cells,[33] should be used and compared as a reference in the future work in order to compete with the cutting-edge technique.

Acknowledgements

The authors appreciate Ina Plock (DLR, Stuttgart) and Suzanne Jacomet (Armines, France) for the SEM and EDS analysis, also acknowledge Anke Lützner (DLR, Stuttgart) for the XPS measurements and Pierre Ilbizian (Armines, France) for the supercritical drying. The research leading to these results has received funding from the European Union's Seventh Framework Programme (FP7/2007–2013) for Fuel Cell and Hydrogen Joint Technology Initiative under Grant No. 621237 (INSIDE) and Grant No. 325239 (NanoCAT).

References

1 M. Carmo, D. L. Fritz, J. Mergel and D. Stolten, *Int. J. Hydrogen Energy*, 2013, **38**, 4901–4934.
2 C. Rozain, E. Mayousse, N. Guillet and P. Millet, *Appl. Catal., B*, 2016, **182**, 153–160.
3 L. C. Seitz, C. F. Dickens, K. Nishio, Y. Hikita, J. Montoya, A. Doyle, C. Kirk, A. Vojvodic, H. Y. Hwang, J. K. Norskov and T. F. Jaramillo, *Science*, 2016, **353**, 1011–1014.
4 H. N. Nong, H. S. Oh, T. Reier, E. Willinger, M. G. Willinger, V. Petkov, D. Teschner and P. Strasser, *Angew. Chem., Int. Ed.*, 2015, **54**, 2975–2979.
5 E. A. Paoli, F. Masini, R. Frydendal, D. Deiana, C. Schlaup, M. Malizia, T. W. Hansen, S. Horch, I. E. L. Stephens and I. Chorkendorff, *Chem. Sci.*, 2015, **6**, 190–196.
6 L. Wang, P. Lettenmeier, U. Golla-Schindler, P. Gazdzicki, N. A. Cañas, T. Morawietz, R. Hiesgen, S. S. Hosseiny, A. S. Gago and K. A. Friedrich, *Phys. Chem. Chem. Phys.*, 2016, **18**, 4487–4495.
7 P. Lettenmeier, L. Wang, U. Golla-Schindler, P. Gazdzicki, N. A. Cañas, M. Handl, R. Hiesgen, S. S. Hosseiny, A. S. Gago and K. A. Friedrich, *Angew. Chem., Int. Ed.*, 2016, **128**, 752–756.
8 S. Cherevko, S. Geiger, O. Kasian, N. Kulyk, J. Grote, A. Savan, B. Ratna, S. Merzlikin, B. Breitbach, A. Ludwig and K. J. J. Mayrhofer, *Catal. Today*, 2016, **262**, 170–180.
9 N. Danilovic, R. Subbaraman, K. C. Chang, S. H. Chang, Y. J. Kang, J. Snyder, A. P. Paulikas, D. Strmcnik, Y. T. Kim, D. Myers, V. R. Stamenkovic and N. M. Markovic, *J. Phys. Chem. Lett.*, 2014, **5**, 2474–2478.

10 N. Danilovic, R. Subbaraman, K. C. Chang, S. H. Chang, Y. Kang, J. Snyder, A. P. Paulikas, D. Strmcnik, Y. T. Kim, D. Myers, V. R. Stamenkovic and N. M. Markovic, *Angew. Chem., Int. Ed.*, 2014, **53**, 14016–14021.
11 G. Chen, S. R. Bare and T. E. Mallouk, *J. Electrochem. Soc.*, 2002, **149**, A1092–A1099.
12 R. Kötz, S. Stucki and B. Carcer, *J. Appl. Electrochem.*, 1991, **21**, 14–20.
13 H. S. Oh, H. N. Nong and P. Strasser, *Adv. Funct. Mater.*, 2015, **25**, 1074–1081.
14 F. Vicent, E. Morallón, C. Quijada, J. L. Vázquez, A. Aldaz and F. Cases, *J. Appl. Electrochem.*, 1998, **28**, 607–612.
15 V. K. Puthiyapura, M. Mamlouk, S. Pasupathi, B. G. Pollet and K. Scott, *J. Power Sources*, 2014, **269**, 451–460.
16 H. S. Oh, H. N. Nong, D. Teschner, T. Reier, A. Bergmann, M. Gliech, J. Ferreira de Araújo, E. Willinger, R. Schloegl and P. Strasser, *J. Am. Chem. Soc.*, 2016, **138**, 12552–12563.
17 H. Du, L. Gan, B. Li, P. Wu, Y. Qiu, F. Kang, R. Fu and Y. Zeng, *J. Phys. Chem. C*, 2007, **111**, 2040–2043.
18 G. Ozouf, G. Cognard, F. Maillard, L. Guétaz, M. Heitzmann and C. Beauger, *ECS Trans.*, 2015, **69**, 1207–1220.
19 L. G. R. A. Santos, K. S. Freitas and E. A. Ticianelli, *Electrochim. Acta*, 2009, **54**, 5246–5251.
20 H. Yano, M. Kataoka, H. Yamashita, H. Uchida and M. Watanabe, *Langmuir*, 2007, **23**, 6438–6445.
21 B. Li, D. C. Higgins, D. Yang, H. Lv, Z. Yu and J. Ma, *Int. J. Hydrogen Energy*, 2013, **38**, 5813–5822.
22 C. Gutsche, C. J. Moeller, M. Knipper, H. Borchert, J. Parisi and T. Plaggenborg, *Electrocatalysis*, 2015, **6**, 455–464.
23 Y. Li, H. Xu, H. Zhao, L. Lu and X. Sun, *J. Appl. Electrochem.*, 2016, **46**, 183–189.
24 G. Ozouf and C. Beauger, *J. Mater. Sci.*, 2016, **51**, 5305–5320.
25 T. J. Schmidt, U. A. Paulus, H. A. Gasteiger and R. J. Behm, *J. Electroanal. Chem.*, 2001, **508**, 41–47.
26 I. Katsounaros, J. C. Meier and K. J. J. Mayrhofer, *Electrochim. Acta*, 2013, **110**, 790–795.
27 M. C. Biesinger, L. W. M. Lau, A. R. Gerson and R. S. C. Smart, *Appl. Surf. Sci.*, 2010, **257**, 887–898.
28 *Handbook of X-ray Photoelectron Spectroscopy*, ed. J. F. Moulder, W. F. Stickle, P. E. Sobol and K. D. Bomben, Physical Electronics, Inc., 1995.
29 J. H. Harreld, W. Dong and B. Dunn, *Mater. Res. Bull.*, 1998, **33**, 561–567.
30 J. C. Slater, *J. Chem. Phys.*, 1964, **41**, 3199.
31 C. L. Green and A. Kucernak, *J. Phys. Chem.*, 2002, **2**, 11446–11456.
32 S. C. F. Araujo, Master degree thesis, University of North Texas, August 2016.
33 N. Cheng, Y. Shao, J. Liu and X. Sun, *Nano Energy*, 2016, **29**, 220–242.

